Supplementary Information

Rivett, DW, and T Bell. Abundance determines the functional role of bacterial phylotypes in complex communities. *Nature Microbiology.*

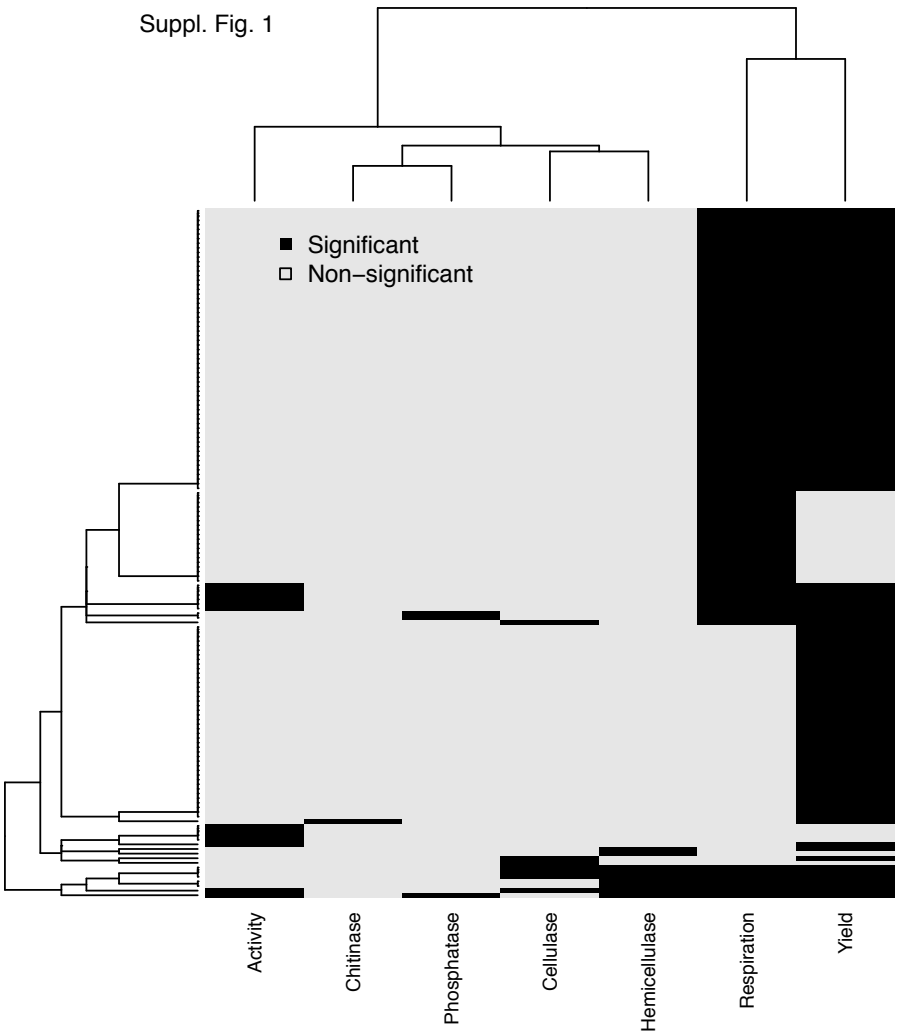

Supplementary Figure 1. Significant associations between phylotype abundance and the functional measurements. Each row is a phylotype, and each column is a functional measurement. Black indicates a significant association (linear regression, $p < 0.05$, no Bonferroni correction) between the phylotype and the functional measurement, while grey indicates no significant association ($p > 0.05$). The data show that phylotypes differed in their associations with the functional measurements. Rows and columns are ordered according their similarity. Functional measurements that have similar phylotype associations are clustered together, and phylotypes with similar patterns of association are clustered together. The marginal trees show the hierarchical clustering of the rows and columns, with phylotypes (rows) or functions (columns) that have similar patterns being clustered together. The associations are the same as those presented in top- and right-hand plot of Figure 2 (n = 753 communities, 522 phylotypes, 7 functional measurements). Phylotypes with no significant associations across all 7 functional measurements were not included in the plot.

Supplementary Figure 2

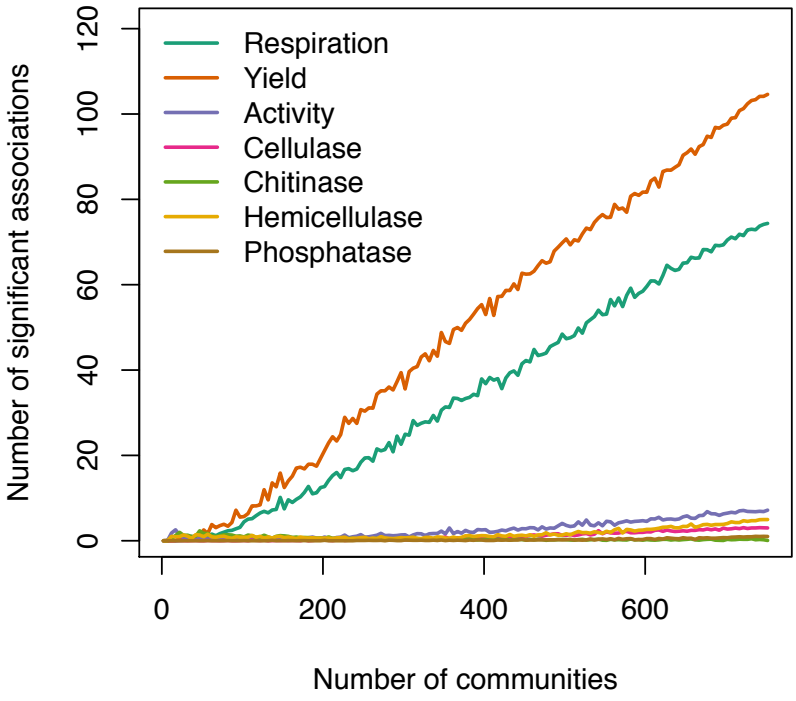

Supplementary Figure 2. Effect of sampling effort on the number of significant associations. We randomly sampled a subset of the n = 753 communities (repeated 30 times) and looked for associations between each phylotype of the 522 phylotypes and the 7 functional measurements according to the one- way analysis described in the methods. Each line is the mean number of associations across the 30 repeats. There tended to be a linear increase in the number of associations discovered, with the exception of chitinase for which we were unable to find any significant associations.

Supplementary Figure 3

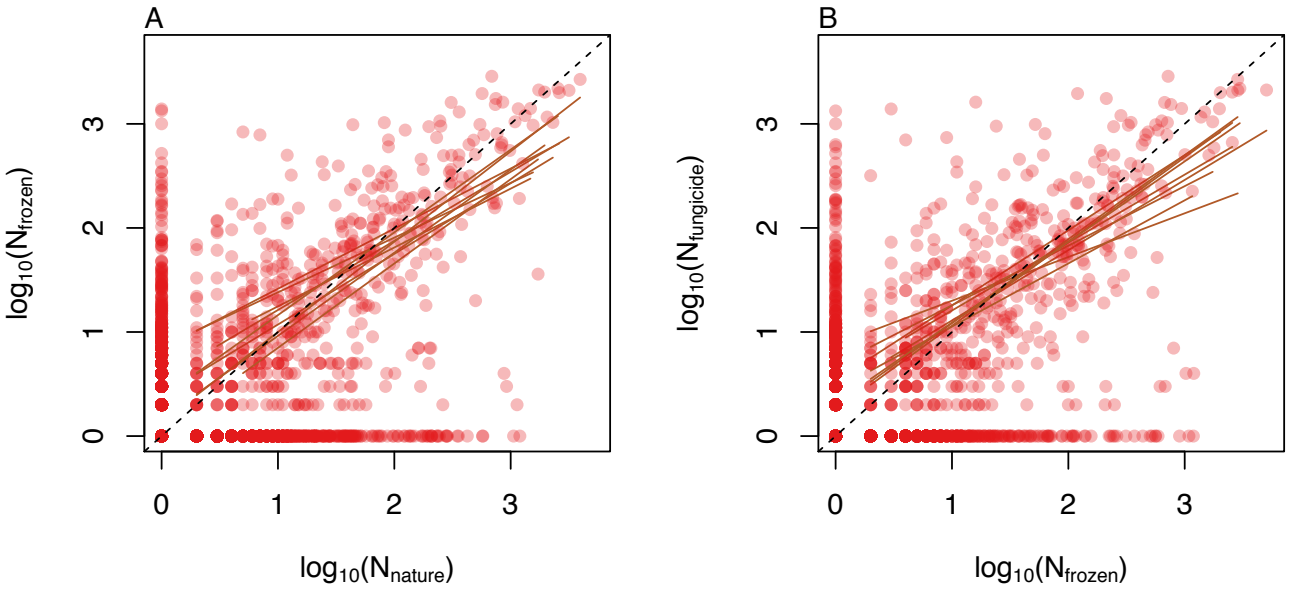

Supplementary Figure 3. Impact of freezing and fungicide treatments on phylotype abundance. We assessed how the common garden methodology (Figure 1) altered the bacterial communities. We sampled n = 9 separate tree-holes. Samples were filtered to remove coarse debris. A subsample was frozen (-80C) and thawed. Both unmanipulated samples ("nature") and frozen samples were inoculated into microcosms with or without cycloheximide ("fungicide"). All conditions were the same as those described in the common garden experiment. We extracted DNA following 7 days of incubation, and sequenced the 16S locus as descried in the Methods. We subsampled 15,000 amplicons at random from each sample. The figure shows the abundance of each of the n = 522 phylotypes in unmanipulated samples (N_{nature}) as a function of their abundance following freezing (N_{frozen}) or following freezing and fungicide application ($N_{fungicide}$). The dashed line is the 1:1 (i.e. where y-axis values = x-axis values). The solid lines are the least squares fit for each individual tree hole. Phylotypes that did not yield any sequences (zero sequences) were excluded from the least square fit. The freezing and application of fungicide impacted the abundance of many phylotypes, with some phylotypes completely eliminated by the procedure. However, the result also shows that, on average across all phylotypes, phylotype abundances before the manipulations were strongly related to their abundances after the manipulations (linear regression, mean R^2= 0.5, mean slope = 0.7, mean p-value = 0.0003).

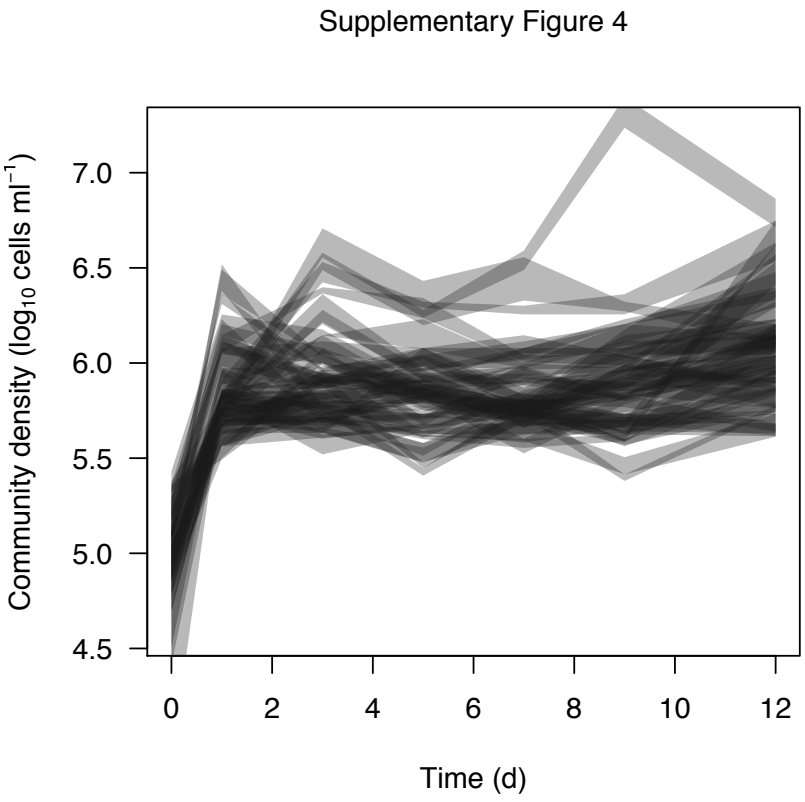

Supplementary Figure 4. Community growth during the common garden experiment. We tracked community abundance over 12 days for n = 32 randomly selected communities. Communities were thawed and aliquoted into microcosms according to the same method for the common garden experiment. We quantified cell densities within the microcosms as described in the functional measurements. The plotted polygons show the standard error around each mean community trajectory (n = 2 technical replicates per community).

Supplementary Figure 5

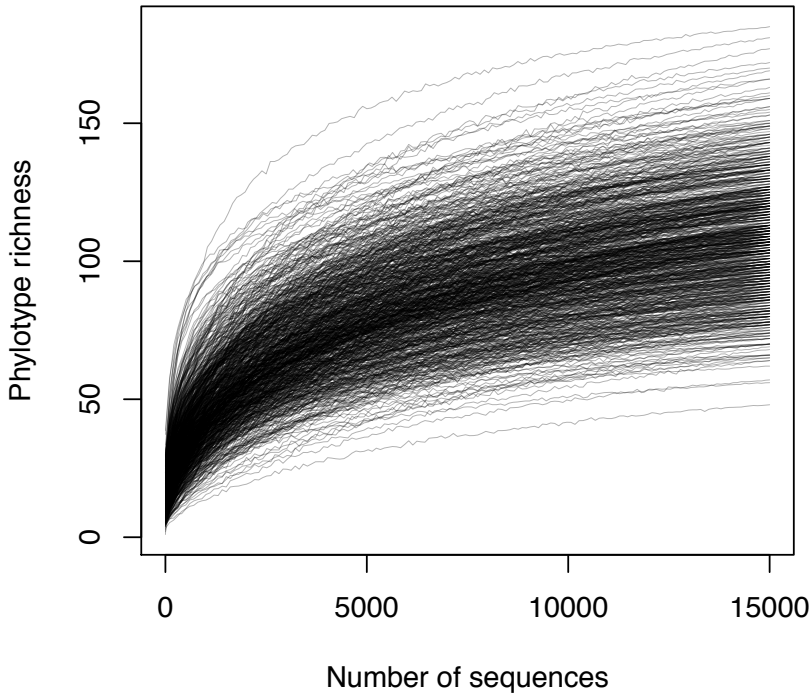

Supplementary Figure 5. Rarefaction curves for the communities. We randomly sampled sequences from each community (n = 753) to characterise the accumulation of phylotypes with increasing sequencing effort. Sequencing effort was normalised across all samples to 15,000 sequences.

Supplementary Figure 6

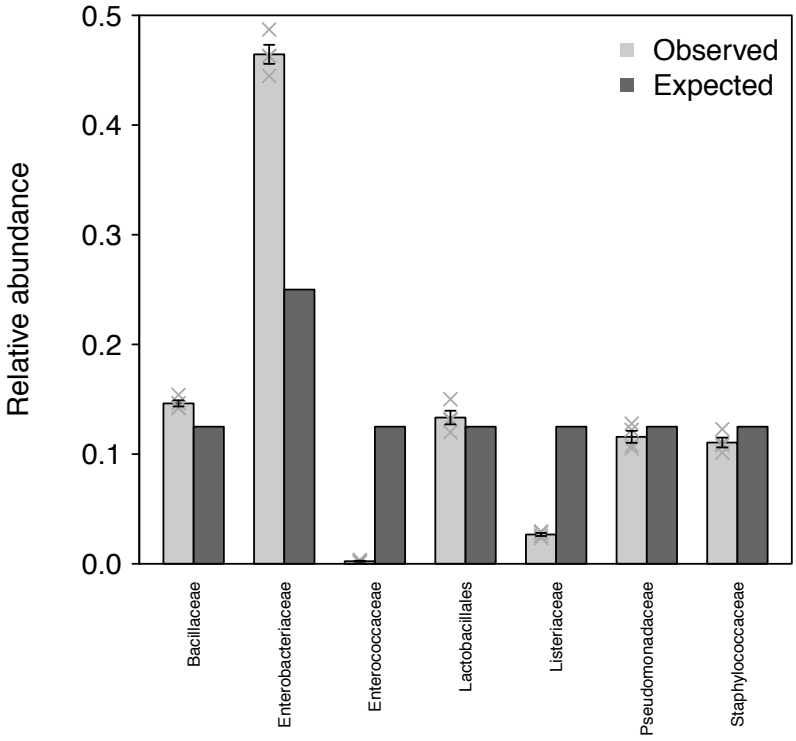

Supplementary Figure 6. Positive controls used to characterise biases in 16S sequencing. We included a standard microbial community (ZymoBIOMICS Microbial Community Standards, Zymo Research) within the sequencing runs to assess for biases in the sequencing methodology (n= 4 replicates of the positive control samples;data from each replicate is shown with an 'x' in the figure). We found that the actual proportion of 16S rRNA reads corresponded to those we obtained via amplicon sequencing, with the main discrepancy observed between members of the Enterobacteriaccae. Observed values are means +/- standard errors.

Supplementary Figure 7

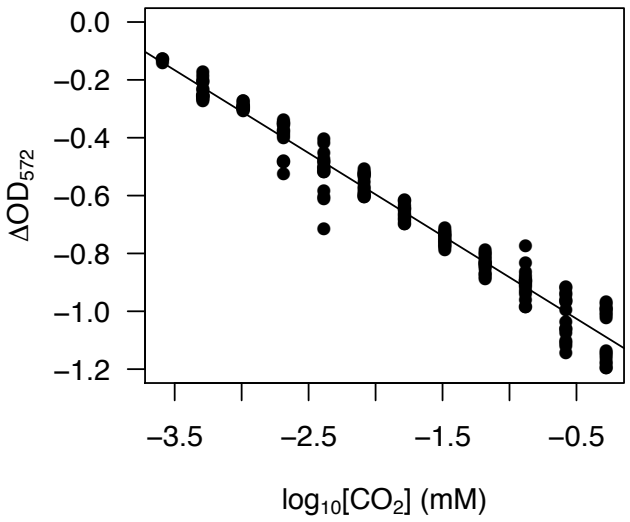

Supplementary Figure 7. MicroResp calibration curve to convert colour change (optical density) to CO_2. In the experiments, respired CO_2 in the microcosms reacted with a pH indicator to produce a colour change. We then quantified this colour change using by measuring the change in optical density at 572 nm. We calibrated the MicroResp absorbance readings by dissolving a known mass of $CaCO_3$ in HCl in sterile microcosms (12 $CaCO_3$ concentrations, n = 16 technical replicates per concentration). The reaction between $CaCO_3$ and HCl produces a known quantity of CO_2 (x axis of figure). The fitted relationship between the change in absorbance after 60 minutes (y axis) and the quantity of CO_2 produced from the chemical reaction was used to quantify CO production in the experimental microcosms. The solid line is the least squares fit: $OD_{572} = -1.169 - 0.286(\log_{10}[CO_2])$, $R^2 = 0.965$, $F_{1, 178} = 4937$, $p < 10^{-16}$).